AIP | Review of Scientific Instruments

The geometric factor of electrostatic plasma analyzers: A case study from the Fast Plasma Investigation for the Magnetospheric Multiscale mission

Glyn A. Collinson, John C. Dorelli, Levon A. Avanov, Gethyn R. Lewis, Thomas E. Moore et al.

Citation: Rev. Sci. Instrum. **83**, 033303 (2012); doi: 10.1063/1.3687021
View online: http://dx.doi.org/10.1063/1.3687021
View Table of Contents: http://rsi.aip.org/resource/1/RSINAK/v83/i3
Published by the American Institute of Physics.

The geometric factor of electrostatic plasma analyzers: A case study from the Fast Plasma Investigation for the Magnetospheric Multiscale mission

Glyn A. Collinson,[1,2,a),b)] John C. Dorelli,[1,b)] Levon A. Avanov,[3,1] Gethyn R. Lewis,[2] Thomas E. Moore,[1] Craig Pollock,[1] Dhiren O. Kataria,[2] Robert Bedington,[2] Chris S. Arridge,[2,4] Dennis J. Chornay,[5,1] Ulrik Gliese,[6,1] Al Mariano,[1] Alexander C. Barrie,[7,1] Corey Tucker,[8,1] Christopher J. Owen,[2] Andrew P. Walsh,[2] Mark D. Shappirio,[1] and Mark L. Adrian[1]

[1]*Heliophysics Science Division, NASA Goddard Space Flight Center, Greenbelt, Maryland 20071, USA*
[2]*Mullard Space Science Laboratory, University College London, Holmbury St. Mary, Surrey, United Kingdom*
[3]*Innovim, 7501 Greenway Center Drive, Maryland Trade Center III, Greenbelt, Maryland 20770, USA*
[4]*The Centre for Planetary Sciences, UCL/Birkbeck, United Kingdom*
[5]*University of Maryland, 7403 Hopkins Avenue, College Park, Maryland 20740, USA*
[6]*SGT, Inc., 7515 Mission Drive, Suite 30, Lanham, Maryland 20706, USA*
[7]*Millennium Engineering and Integration, 2231 Crystal Dr., Arlington, Virginia 22202, USA*
[8]*Global Science and Technology Inc., 7855 Walker Drive, Greenbelt, Maryland 20770, USA*

(Received 3 October 2011; accepted 1 February 2012; published online 21 March 2012; publisher error corrected 29 March 2012)

We report our findings comparing the geometric factor ($\mathbb{GF}$) as determined from simulations and laboratory measurements of the new Dual Electron Spectrometer (DES) being developed at NASA Goddard Space Flight Center as part of the Fast Plasma Investigation on NASA's *Magnetospheric Multiscale* mission. Particle simulations are increasingly playing an essential role in the design and calibration of electrostatic analyzers, facilitating the identification and mitigation of the many sources of systematic error present in laboratory calibration. While equations for laboratory measurement of the $\mathbb{GF}$ have been described in the literature, these are not directly applicable to simulation since the two are carried out under substantially different assumptions and conditions, making direct comparison very challenging. Starting from first principles, we derive generalized expressions for the determination of the $\mathbb{GF}$ in simulation and laboratory, and discuss how we have estimated errors in both cases. Finally, we apply these equations to the new DES instrument and show that the results agree within errors. Thus we show that the techniques presented here will produce consistent results between laboratory and simulation, and present the first description of the performance of the new DES instrument in the literature. © *2012 American Institute of Physics*. [http://dx.doi.org/10.1063/1.3687021]

I. INTRODUCTION

The geometric factor ($\mathbb{GF}$) of an electrostatic plasma analyzer (ESA) facilitates the conversion of the number of particles detected by the analyzer during an integration time to the ambient plasma differential energy flux (from which an equivalent phase space density may be estimated).[1] Reliable and accurate determination of the $\mathbb{GF}$, however, is a non-trivial exercise, since there are many sources of random and systematic experimental error to take into account. Simulations of the particle trajectories as they pass through the optics to the detector thus play an essential part in the identification and mitigation of systematic experimental errors—e.g., optics misalignment,[2] electronic noise, variations in detector efficiencies, etc.—that are often specific to the particular laboratory setup and difficult to track down. However, particle simulations are often run under conditions that differ substantially from those in the laboratory and can introduce errors of their own.[3]

While techniques and equations for laboratory measurement of the $\mathbb{GF}$ have been described in the literature,[4–6] these are not readily applicable to simulation due to the often significant differences between the setup in the laboratory and the assumptions made for simulation. However, for direct comparison between laboratory and simulation there must be complete confidence that the equations used to calculate the $\mathbb{GF}$ are mathematically equivalent. Otherwise, it is not possible to ensure that any discrepancies or agreements are genuine. While many previous groups have made use of simulations to calculate or verify their $\mathbb{GF}$ measurements,[7–11] to our knowledge, the details of these comparisons have not been presented in the literature in a general and systematic way.

The purpose of this paper is two-fold. First to describe a general formalism for comparing simulated and measured geometric factors of top hat analyzers. Second, to describe our application of this formalism to the $\mathbb{GF}$ determined from computer simulations and laboratory measurements of the new Dual Electron Spectrometer (DES) (shown in Figure 1) being developed at NASA Goddard Space Flight Center (GSFC) as part of the Fast Plasma Investigation (FPI) to be flown on NASA's upcoming *Magnetospheric Multiscale* (MMS) mission. Starting from first principles, we derive generalized expressions for the determination of the $\mathbb{GF}$ in simulation and laboratory, and discuss how we have estimated errors in both

[a)]Electronic mail: glyn.a.collinson@nasa.gov.
[b)]G. A. Collinson and J. C. Dorelli contributed equally to this work.

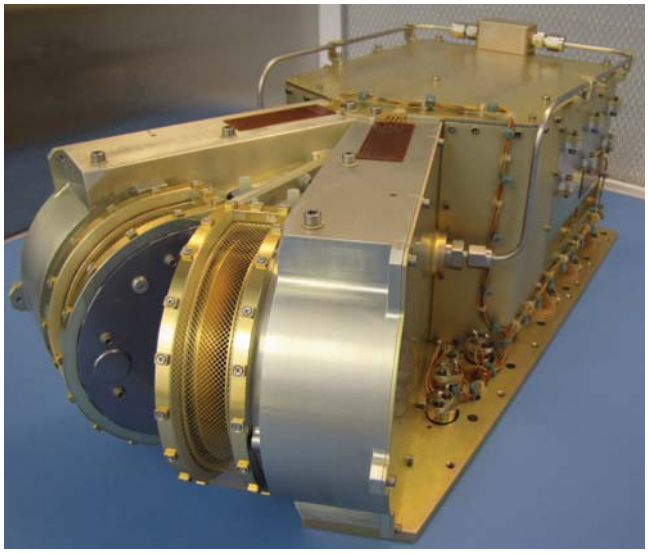

FIG. 1. (Color Online) The engineering test unit (ETU) of the new Dual Electron Spectrometer (DES) for NASA's *Magnetospheric Multiscale* (MMS) Mission.

cases. We then apply these equations to example data from the new DES, and thus demonstrate that the results agree to within identified errors.

The paper is organized as follows:

1. In Sec. II, we present the derivation of a generalized $\mathbb{GF}$ equation.
2. In Sec. III, we outline a suggested methodology for the computer simulation of ESAs. Then we derive an equation for $\mathbb{GF}$ specifically for computer simulation and discuss how we have estimated the error in its measurement.
3. In Sec. IV, we derive an equation for the determination of the $\mathbb{GF}$ from laboratory calibration, and again discuss how we have estimated the error.
4. Finally, in Sec. V, we show an example of how these equations have been used to calculate the $\mathbb{GF}$ of the engineering test unit (ETU) of the new DES.

Thus we show that the techniques presented here will produce consistent results between laboratory and simulation, and present the first description of the performance of the DES in the literature.

II. THE GEOMETRIC FACTOR

The *"geometric factor"* is a historical phrase that is used to denote something that is not entirely based on instrument geometry. In reality, it is used as a catch-all term that allows conversion between counts on the detector to phase space density, and as such also includes other elements not related to the geometry of the instrument such as the efficiency of the detector (to be discussed later).[5,8,10,12,13]

A. Mathematical definition

We will now derive a generalized equation for the $\mathbb{GF}$ from first principles. To begin, following Johnstone *et al.*,[5] we introduce the concept of an *"instrument response function"* ($\mathbb{R}$). This is a notional mathematical construct that relates how the instrument responds when a flux of particles is incident upon it. It describes the effects of the ESA optics as well as any non-optical elements (such as detection efficiency). These additional factors may be dependent on the energy of the particle, and will later be referred to as "$q(E)$".

At the time of writing, the most commonly used method of particle detection is by using a micro-channel plate (MCP)[14] as a charge amplifier, resulting in an electron shower that is detected as a charge deposition on an anode by read-out electronics.[15] The anode is often sub-divided into segments, giving the instrument angular sensitivity. A plasma analyzer therefore accumulates counts on each anode or other such angular pixel (i) and in each energy bin (j). Some types of ESA use electrostatic deflector plates,[16–18] to sweep the field of view of the instrument over a range of angles. In this case, the plasma analyzer also accumulates counts at each deflection state (k).

We thus begin by defining the instrument response function $\mathbb{R}_{ijk}(\mathbf{v}, \mathbf{v}_0, \mathbf{x}, t)$ such that the number of particles detected (for a given mass to charge ratio), C_{ijk} is given by Eq. (1), as first defined by Johnstone *et al.*,[5]

$$C_{ijk} \equiv -\int_0^\tau dt \int d\mathbf{A} \cdot \int_{v-} d\mathbf{v}\, \mathbf{v}\, \mathbb{R}_{ijk}(\mathbf{v}, \mathbf{v}_0, \mathbf{x}, t)\, f(\mathbf{v}, \mathbf{x}, t), \tag{1}$$

where $\mathbb{R}_{ijk}(\mathbf{v}, \mathbf{v}_0, \mathbf{x}, t)$, and the particle distribution function, $f(\mathbf{v}, \mathbf{x}, t)$ are integrated over the particle velocities into the aperture, the area of the aperture, and the period of accumulation (τ). In general, for a plasma containing multiple ion species, $f(\mathbf{v}, \mathbf{x}, t)$ might be a sum over all of those species with charge to mass ratio selected by $\mathbb{R}_{ijk}$. However, the experiments we describe in this paper do not suffer form this ambiguity because we are measuring only electrons. The independent variable is the single-particle velocity space coordinate ($\mathbf{v}$), and $d\mathbf{A}$ is a differential area element of the detector aperture (with direction parallel to the local outward normal to the aperture). $v-$ indicates that integration is over that region of velocity space ($\mathbf{v} \cdot d\mathbf{A} < 0$). $\mathbf{v_0}$ is a vector parameter which describes the shape of the instrument response function with a global maximum at $\mathbf{v} = \mathbf{v}_0$.

Measurements of the response of a space plasma analyzer are made in terms of energy and angle, rather than velocity and position. It is therefore convenient to introduce the coordinate system depicted in Figure 2. The velocity space is represented by spherical-polar coordinates (E, θ, ϕ), where E is the single-particle energy, $E = mv^2/2$, θ is the *particle elevation*, and ϕ is the *particle azimuth*. To proceed further, the following assumptions are made:

1. The aperture area can be approximated as a rectangle with area $A_{ij} \equiv \Delta Y \Delta Z$ whose normal is in the $-$X direction.
2. The integration time is small enough so that the incident particle phase space density is constant over the integration time.

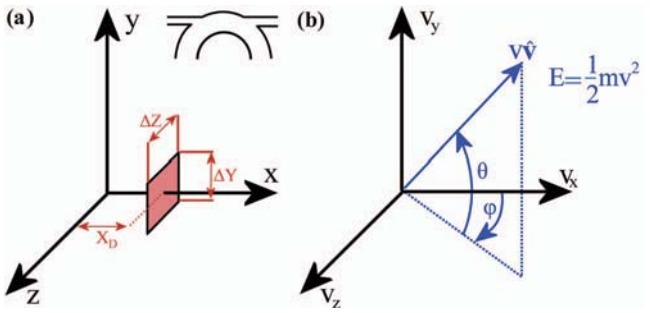

FIG. 2. (Color Online) Space co-ordinate system with respect to an analyzer (panel a) and spherical-polar single-particle velocity space coordinate system (panel b). The rectangle in panel a (coloured red online) shows the detector aperture, here approximated as a rectangle with area A_{ij}, whose centroid is located at (X_D, 0, 0). The right panel shows the coordinate system used to describe the single-particle velocity distribution function, $f(E, \theta, \phi)$, at an arbitrary location on the instrument.

3. A_{ij} is small enough so that the incident particle phase space density is constant over the detector aperture.

When the above conditions are satisfied, Eq. (1) becomes:

$$C_{ijk} \equiv \frac{2\tau A_{ij}}{m^2} \int_0^\infty dE\, E \int_{-\frac{\pi}{2}}^{\frac{\pi}{2}} d\theta\, \cos^2\theta \int_{-\frac{\pi}{2}}^{\frac{\pi}{2}} d\phi\, \cos\phi \times \bar{\mathbb{R}}_{ijk}(E, \theta, \phi; E_0, \theta_0, \phi_0)\, f(E, \theta, \phi), \quad (2)$$

where

$$d\mathbf{v} = v^2 dv d\theta\, \cos\theta d\phi$$
$$dv = \frac{dE}{\sqrt{2mE}}$$
$$v = \sqrt{\frac{2E}{m}}$$
$$d\mathbf{A}\cdot\mathbf{v} = dAv\cos\theta\cos\phi = dYdZv\cos\theta\cos\phi.$$

Next we define the following space–time averaged detector response, $\bar{\mathbb{R}}_{ijk}$:

$$\bar{\mathbb{R}}_{ijk}(E, \theta, \phi; E_0, \theta_0, \phi_0) \equiv \frac{1}{A_{ij}\tau} \int_0^\tau dt \int_{-\Delta Y/2}^{\Delta Y/2} dY \int_{-\Delta Z/2}^{\Delta Z/2} dZ \times \mathbb{R}_{ijk}((E, \theta, \phi; E_0, \theta_0, \phi_0), Y, Z, t), \quad (3)$$

where E_0, θ_0, and ϕ_0 are the spherical polar coordinates corresponding to vector v_0 in Eq. (1) (the location of the global maximum of the response function). Now we may define the generalized definition of the geometric factor, $\mathbb{GF}_{ijk}$ used in this paper as

$$\mathbb{GF}_{ijk} \equiv \frac{A_{ij}}{E_0^2} \int_0^\infty dE\, E \int_{-\frac{\pi}{2}}^{\frac{\pi}{2}} d\theta\, \cos^2\theta \int_{-\frac{\pi}{2}}^{\frac{\pi}{2}} d\phi\, \cos\phi\, \bar{\mathbb{R}}_{ijk} \times (E, \theta, \phi; E_0, \theta_0, \phi_0). \quad (4)$$

Note that there exist some phase space structures on scales comparable or smaller to the response function, e.g., the Solar Wind Strahl.[19] In such cases, one needs to deconvolve the integral in Eq. (1) in order to compute the phase space density from the measured count rate. If the phase space density $f(E, \theta, \phi)$ is approximately constant over the detector response, then Eq. (2) can be written as follows:

$$C_{ijk} \equiv \frac{2\tau A_{ij}}{m^2} f(E, \theta, \phi) \int_0^\infty dE\, E \int_{-\frac{\pi}{2}}^{\frac{\pi}{2}} d\theta\, \cos^2\theta \times \int_{-\frac{\pi}{2}}^{\frac{\pi}{2}} d\phi\, \cos\phi\, \bar{\mathbb{R}}_{ijk}(E, \theta, \phi; E_0, \theta_0, \phi_0), \quad (5)$$

Then we may substitute the definition of the $\mathbb{GF}$ (4) into Eq. (5) to approximate $\mathbb{GF}$ as below as

$$C_{ijk} \approx \frac{2\tau A_{ij}}{m^2} f(E, \theta, \phi)\, \mathbb{GF}_{ijk} \frac{E_0^2}{A_{ij}}. \quad (6)$$

With some minor re-arrangement and cancellation, we arrive at Eq. (7).

$$C_{ijk} \approx \frac{2E_0^2}{m^2}\, \mathbb{GF}_{ijk}\, \tau f(E_0, \theta_0, \phi_0) \quad (7)$$

This in turn allows conversion between C_{ijk} and the differential energy flux, $J(E, \theta, \phi, \mathbf{x})$, as in Eq. (8).

$$C_{ijk} \approx \mathbb{GF}_{ijk}\ \tau\ J(E, \theta, \phi, \mathbf{x}). \quad (8)$$

The units of $\mathbb{GF}$ are cm^2 sr eV/eV, where eV/eV is included to indicate that it is a function of both the range of energies of the particles and a central energy of the instrument transmission bandpass.

B. Speed based definition of the Geometric Factor

While we have chosen to work in energy, and many studies[6,10,16,20] of ESAs also cite the $\mathbb{GF}$ in terms of energy (as in Eq. (8)), others (including the afore mentioned Johnstone *et al.*,[5]) calculate it in terms of speed[12,21] (see Eq. (9)).

$$\mathfrak{GF}_{(s)ijk} \equiv \frac{A_{ij}}{v_0^4} \int_0^\infty dv\, v^3 \int_{-\frac{\pi}{2}}^{\frac{\pi}{2}} d\theta\, \cos^2\theta \int_{-\frac{\pi}{2}}^{\frac{\pi}{2}} d\phi\, \cos\phi \times \bar{\mathbb{R}}_{ijk}(v, \theta, \phi). \quad (9)$$

This leads to the following speed-based definition of the Geometric Factor ($\mathfrak{GF}_{(s)ijk}$),

$$C_{ijk} \approx \mathfrak{GF}_{(s)ijk}\ f(v, \theta, \phi)\ v^4\tau. \quad (10)$$

It is important to note that this speed-based definition of the of the Geometric Factor ($\mathfrak{GF}_{(s)ijk}$) is exactly half that of the energy-based definition $\mathbb{GF}_{ijk}$, leading to a factor of two discrepancy, as in Eq. (11). We emphasize this because both of these definitions occur prevalently in the literature,[13]

$$\mathbb{GF}_{ijk} = 2\,\mathfrak{GF}_{(s)ijk}. \quad (11)$$

This is a result of the conversion between energy (Eq. (2)) and speed (Eq. (9)) using the following:

$$E_0 = mv_0^2/2,$$
$$dE = mv\, dv. \quad (12)$$

Thus there is no single and unified definition of the $\mathbb{GF}$ in the literature, and the choice of which is used comes down

to personal preference. However, since the conflicting definitions give conflicting results, it is important to clarify which definition has been used when comparing laboratory and simulation, or when reporting the response of an instrument.

III. DETERMINATION OF GEOMETRIC FACTOR THROUGH COMPUTER SIMULATION

In this section, we use our generalized $\mathbb{GF}$ Eq. (4) to derive an equation for the calculation of the $\mathbb{GF}$ through computer simulations. We then discuss how we have estimated the error in our simulations of $\mathbb{GF}$ for the MMS-DES.

Computer simulation reveals the idealized properties of an ESA, and is now used ubiquitously throughout the community for the purposes of instrument design,[22–25] modification and optimization,[10] and to aid in post-launch calibration.[8,20] There is, therefore, a strong need for a generalized description of how to determine the $\mathbb{GF}$ of any ESA using computer simulation so that the answer will be consistent with that determined through laboratory calibration. In this section, we present such a description, including a derivation of an equation for the computational determination of the $\mathbb{GF}$ from simulation.

A. Description of Monte Carlo simulation method

When performing computer modelling of an ESA, a particle "beam" is launched at some position upstream of the detector aperture. An effective approach is to draw particle energies and elevation angles from a uniform random number generator with ranges $\Delta E_B \equiv E_{\max} - E_{\min}$ and $\Delta\theta_B \equiv \theta_{\max} - \theta_{\min}$ (see Figure 3). The particles are uniformly distributed over a source rectangle in the $Y - Z$ plane with area $\Delta Y_B \times \Delta Z_B$; the centroid of the rectangle is located at $(X_B, 0, Z_B)$. All of the particles are launched with $\phi = 0$.

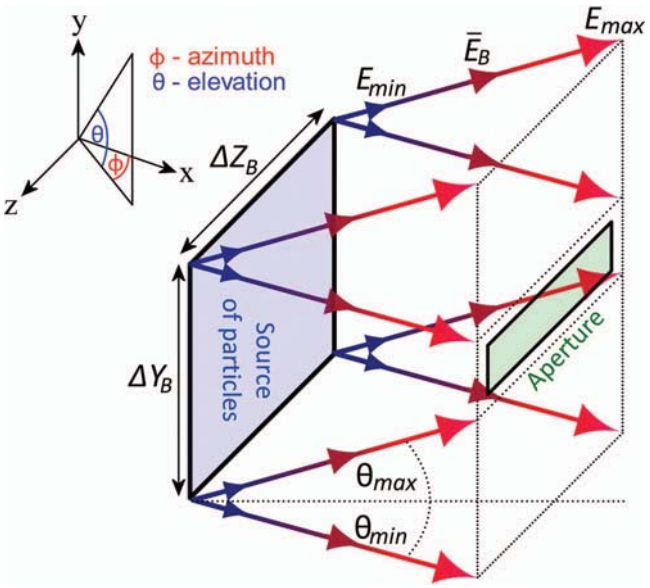

FIG. 3. (Color Online) Schematic showing our suggested methodology for flying particles in a computer simulation.

The values of $E_{\max}$, $E_{\min}$, $\theta_{\max}$, $\theta_{\min}$ must be selected to ensure that the entire energy and angular bandpass of the instrument is covered. Similarly, the position and area of the source of particles (blue rectangle, Figure 3) should be selected to cover the whole area of the simulated instrument over which particles may be transmitted to the detector (green rectangle, Figure 3). This may or may not require covering the whole aperture, depending on the type and design of ESA. The rectangular source should be large enough to ensure that particles fired from the top ($y_{\max}$) with angle $\theta_{\min}$ and from the bottom ($y_{\min}$) with angle $\theta_{\max}$ will cover the limits of the aperture. Therefore, the closer the source of the particles to the aperture, the smaller the area that the source of particles will have to be in order to cover it.

We use a commercially available software package to calculate the electric potential distribution inside the instrument and perform ray-tracing calculations, although some groups choose to use their own software. The randomly generated charged particles traverse the ESA, with a certain number striking the simulated "detector". Charged particles are flown one at a time. The state of each particle is recorded twice; the first time upon its creation, and the second time when it either hits an electrode or leaves the simulation space. On these two occasions (start and stop), the following information is recorded: Position *(x, y, z)*, direction of movement *(Azimuth—ϕ, Elevation—θ)*, and Kinetic Energy *(KE)*.

The main source of error in a simulation should be the statistics of the number of particles fired. To estimate the error attributed to this, we run each simulation multiple times. The $\mathbb{GF}$ (and all other instrument parameters such as energy resolution, analyzer constant, etc.[10]) calculated independently for each simulation, so that a mean and standard deviation can be taken. We have found that the easiest way to achieve this is by running a single long simulation and subdividing the data set. The data set should be "sieved" so that only those particles that have struck the simulated detector are considered. The total number of particles flown (N_{in}) and the number that strike the detector (C_{ijk}) are recorded. The peak of the energy acceptance bandpass (E_0) of the ESA is then calculated as part of our data analysis.

B. An equation for determining $\mathbb{GF}$ through computer simulation

We now show how the measured values of N_{in}, C_{ijk}, and E_0 (along with the variables shown in Figure 3) may be used to determine the $\mathbb{GF}$ of any ESA through computer simulation.

We can write the phase space density describing the simulated particle distribution as follows:

$$f(E,\theta,\phi) = \begin{cases} f_0\,\delta(\phi) & \text{if } \begin{pmatrix} E_{\min} < E < E_{\max} \\ \theta_{\min} < \theta < \theta_{\max} \end{pmatrix} \\ 0 & \text{otherwise,} \end{cases} \tag{13}$$

where f_0 is a constant, and $\delta(\phi)$ is the Dirac delta function. Let N_{in} be the total number of simulated particles launched during

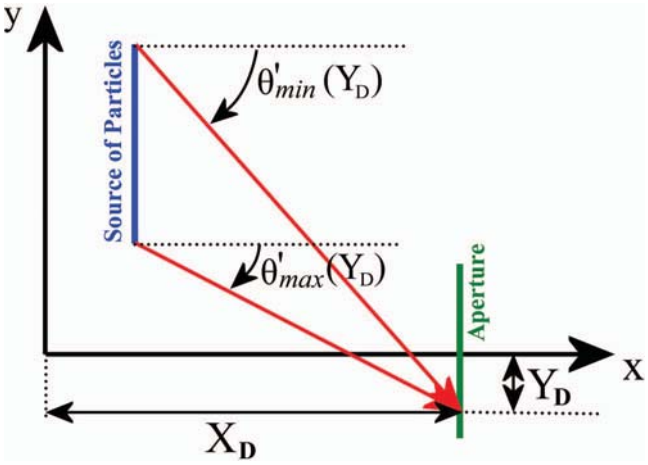

FIG. 4. (Color Online) This figure illustrates the geometry of the simulated particle source projected into the $X-Z$ plane. The line labeled "Source of Particles" (coloured blue online) represents the particle source, which is a rectangle with area $Z_B \times Y_B$ over which the particles' initial positions are uniformly distributed. The arrows leading from it (red online) show two particle trajectories which intersect a point on the detector aperture (green online). Note that only particles with elevations in the range $\theta'_{\min}(Y_D) \le \theta \le \theta'_{\max}(Y_D)$ intersect the detector aperture at location Y_D.

accumulation time τ:

$$N_{in} = \frac{2\tau\,\Delta Y_B \Delta Z_B}{m^2}\int_{E_{\min}}^{E_{\max}} dE\,E \int_{\theta_{\min}}^{\theta_{\max}} d\theta \cos^2\theta \times \int_{-\frac{\pi}{2}}^{\frac{\pi}{2}} d\phi \cos\phi f(E,\theta,\phi). \quad (14)$$

To compute the number of simulated particles which strike the MCP in time τ, we must map the phase space density (13) from the source rectangle (blue line in Figure 4) to the detector aperture (green line in Figure 4). Using Liouville's theorem, which states that the phase space density is constant along particle trajectories, and by assuming the particle trajectories are straight lines, the phase space density at the detector aperture can be given by Eq. (15),

$$f_A(E,\theta,\phi) = \begin{cases} f_0\,\delta(\phi) & \text{if} \begin{pmatrix} E_{\min} < E < E_{\max} \\ \theta'_{\min}(Y_D) < \theta < \theta'_{\max}(Y_D) \end{pmatrix} \\ 0 & \text{otherwise.} \end{cases} \quad (15)$$

Note that the incident phase space density varies, in general, over the surface of the aperture, since the particle elevation limits, $\theta'_{\min}(Y_D)$ and $\theta'_{\max}(Y_D)$, depend on the Y_D coordinate on the aperture. However, so long as the particle elevation limits of the source distribution (13) are chosen so that $\theta'_{\min}(Y_D)$ and $\theta'_{\max}(Y_D)$ are well outside the detector response for all Y_D, we may replace the θ' limits by the constant (independent of Y_D) limits given in Eq. (13) and use Eq. (2) to compute the number of particles which strike the simulated detector. Thus, substituting Eq. (13) into Eq. (2), Eq. (16) may be derived,

$$C_{ijk} = \frac{2A_{ij}}{m^2}\int_{E_{\min}}^{E_{\max}} dE\,E \int_{\theta_{\min}}^{\theta_{\max}} d\theta \cos^2\theta \times \bar{\mathbb{R}}_{ijk}(E,\theta,\phi;E_0,\theta_0,\phi_0)\,f_0. \quad (16)$$

The number of particles launched in the simulation, N_{in}, is given by

$$N_{in} = \frac{2\Delta Y_B \Delta Z_B}{m^2}\int_{E_{\min}}^{E_{\max}} dE\,E \int_{\theta_{\min}}^{\theta_{\max}} d\theta \cos^2\theta f_0 = \frac{2\Delta Y_B \Delta Z_B \bar{E}_B \cos^2\bar{\theta}_B \Delta E_B \Delta\theta_B f_0}{m^2}, \quad (17)$$

where $\bar{E}_B \equiv (E_{\min}+E_{\max})/2$, and $\bar{\theta} \equiv (\theta_{\min}+\theta_{\max})/2$, and we have assumed that $\Delta\theta_B$ and $\Delta\phi$ are small enough so that $\sin\Delta\theta_B \approx \Delta\theta_B$ and $\sin\Delta\phi \approx \Delta\phi$. Dividing Eq. (16) by Eq. (17), we arrive at the following:

$$\frac{C_{ijk}}{N_{in}} = \frac{A_{ij}}{\Delta Y_B \Delta Z_B \bar{E}_B \cos^2\bar{\theta}_B \Delta E_B \Delta\theta_B} \times \int_{E_{\min}}^{E_{\max}} dE\,E \int_{\theta_{\min}}^{\theta_{\max}} d\theta \cos^2\theta \times \bar{\mathbb{R}}_{ijk}(E,\theta,\phi;E_0,\theta_0,\phi_0). \quad (18)$$

If we assume that the detector response has the following phi dependence:

$$\bar{\mathbb{R}}_{ijk}(E,\theta,\phi;E_0,\theta_0,\phi_0) = \begin{cases} \bar{\mathbb{R}}_{ijk}\begin{pmatrix} E,\theta,0;\ldots \\ \ldots E_0,\theta_0,\phi_0 \end{pmatrix} & \text{if}\,(\phi_{\min} < \phi < \phi_{\max}) \\ 0 & \text{otherwise}, \end{cases} \quad (19)$$

where $\Delta\phi \equiv \phi_{\max} - \phi_{\min}$ is the instrument azimuthal pixel width, then Eq. (18) can be written as follows:

$$\frac{C_{ijk}}{N_{in}} = \frac{A_{ij}}{\Delta Y_B \Delta Z_B \bar{E}_B \cos^2\bar{\theta}_B \Delta E_B \Delta\theta_B \Delta\phi} \times \int_{E_{\min}}^{E_{\max}} dE\,E \int_{\theta_{\min}}^{\theta_{\max}} d\theta \cos^2\theta \int_{\phi_{\min}}^{\phi_{\max}} d\phi \cos\phi \times \bar{\mathbb{R}}_{ijk}(E,\theta,\phi;E_0,\theta_0,\phi_0). \quad (20)$$

Thus, if the incident simulated particle beam is broad enough to cover the full detector response, we can use the generalized equation for $\mathbb{GF}$ (4) to rewrite Eq. (20),

$$\frac{C_{ijk}}{N_{in}} = \frac{E_0^2 \mathbb{GF}_{ijk}}{\Delta Y_B \Delta Z_B \bar{E}_B \cos^2\bar{\theta}_B \Delta E_B \Delta\theta_B \Delta\phi}. \quad (21)$$

We thus finally arrive at an expression for the geometric factor from computer simulation (22). Note that only C_{ijk} and E_0 are products of the simulation and all other variables are known inputs,

$$\mathbb{GF}'_{ijk} = \frac{C_{ijk}\Delta Y_B \Delta Z_B \bar{E}_B \cos^2\bar{\theta}_B \Delta E_B \Delta\theta_B \Delta\phi}{N_{in} E_0^2}. \quad (22)$$

The number of incident particles is given by N_{in}, the number that strike the simulated detector is C_{ijk}, $\bar{E}_B$ is the average incident particle energy, ΔE_B and $\Delta\theta_B$ are the energy and angular widths of the incident "beam", and $\Delta Y_B \Delta Z_B$ is the area of the rectangle over which particles are launched. Since simulated particles are "fired" from a single azimuthal angle, $\Delta\phi$ is dependent on the goal of the study. If the subject of interest

is the $\mathbb{GF}$ per anode, then $\Delta\phi$ is defined to be the azimuthal angle covered by each anode. If the goal is to determine the total $\mathbb{GF}$ for a 360° azimuthal field of view of the whole analyzer, then $\Delta\phi$ is defined to be 2π.

It is imperative to note that while Eq. (22) gives the idealized geometrical response of an ESA, this will not take into account any non-geometrical instrument effects mentioned previously (such as detection efficiency, etc.). These will be dependent on the type and design of the specific instrument (type of detector used, transparency of any grids, etc). To account for this, we define $q(E)$, being the ratio at a given energy (E) between the number of particles detected in an idealized case (N_{ideal}) and the number of particles actually detected (N_{actual}) owing to these effects,

$$q(E) = \frac{N_{actual}(E)}{N_{ideal}(E)}. \tag{23}$$

We will shortly address how $q(E)$ may be estimated. Thus, we refer to the idealized best-case geometric response (Eq. (22)) as $\mathbb{GF}'_{ijk}$, and define the true Geometric Factor, allowing direct conversion between particles detected and particles incident as $\mathbb{GF}_{ijk}$ below in Eq. (24),

$$\mathbb{GF}_{ijk} = \frac{C_{ijk}\Delta Y_B \Delta Z_B \bar{E}_B \cos^2\bar{\theta}_B \Delta E_B \Delta\theta_B \Delta\phi \; q(E)}{N_{in}E_0^2}. \tag{24}$$

When reporting any $\mathbb{GF}$ derived through computer simulation, it is therefore important to indicate whether or not an estimated $q(E)$ has been included, and what value has been used.[8,26]

C. Main sources of error in the computer simulation of ESAs

1. Estimation of percentage of particles detected—q(E)

In this section, we show an example of how we have estimated $q(E)$ for the MMS DES-ETU. There are two contributing components.

First, the instrument has three grids through which particles must travel; two on the outside of the aperture (seen in Figure 1), and one separating the optics from the MCP so that a pre-acceleration voltage may be applied to the electrons. These grids are each 90% transparent, and thus the total particle throughput will be reduced to ~73% (~0.9^3) of what it would have been had the grids been absent.

The second component is the efficiency of the detector. The method used by the DES to detect particles is through the use of an MCP charge amplifier, and the detection of the resulting electron shower on an anode by read-out electronics. As a rough first approximation, the efficiency of an MCP can be taken to be ≈60 → 65%. For a more thorough estimation, it must be considered that the efficiency of an MCP varies with the incident particle energy.[27,28] The dashed line on Figure 5 shows how MCP efficiency varies with energy for a typical MCP stack.[14] We have estimated a maximum efficiency of 80% for the DES-ETU based on laboratory measurement. The variation with energy in Figure 5 is according to the secondary electron emission properties of lead glass as described by Goruganthu and Wilson.[29] Note that the efficiency of an MCP for electrons falls off below 200 eV. However, the DES uses a pre-acceleration voltage of 200 V to negate this, and as such there is no such drop in Figure 5. The solid line on Figure 5 shows how the total percentage of particles detected $q(E)$ is expected to vary with energy, taking into account the aforementioned effect of the grids.

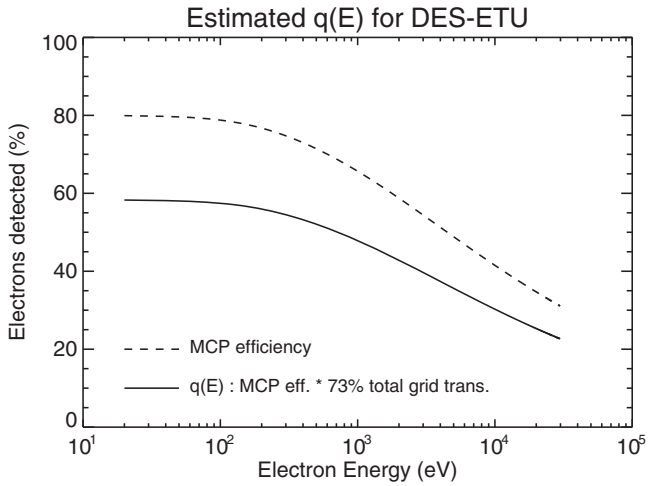

FIG. 5. Plot of MCP efficiency (dashed line) and total percentage of particles detected ($q(E)$ – solid line) vs. energy of electron for the MMS DES-ETU.

For an even more thorough estimation of the efficiency of the MCP, one can take into account that the efficiency is also a function of the angle between the incoming particle trajectory and the channel axis direction.[30] There are several ESA studies which also discuss this in greater detail.[20,26] Additionally, the gain of an MCP decreases over its lifetime,[14,31] which will reduce $q(E)$. We have assumed that the MCP is not saturated, or else an increase in particle flux would not result in an increase in counts.

2. Miscellaneous simulation effects

When simulating an ESA, there are several possible sources of inaccuracy, which include:

1. The number of total particles flown (described previously).
2. The spatial resolution and accuracy of the geometry under study.[3]
3. The resolution and accuracy of the calculation of the fields.
4. The spatial resolution of the particle trajectory integrations.

Since a balance must always be struck between the accuracy of a simulation and the time required for it to run, we have used convergent studies to optimize the four above cases. For example, for spatial resolution (case 2), we performed several simulations at increasing resolution and confirmed that the solutions converged towards a single answer. It should also be noted that our method does not at present simulate secondary electron emission[32] or primary electron scattering.[33,34] These

effects can generate unwanted signal noise, the degree of which is dependent on the design of the instrument.[23,24]

IV. DETERMINATION OF $\mathbb{GF}$ THROUGH LABORATORY MEASUREMENT

In this section, we use our generalized $\mathbb{GF}$ Eq. (4) to derive an equation for the calculation of the $\mathbb{GF}$ in the laboratory.[5,12] We then discuss potential sources of error, and present an example of how we have estimated the error in our measurements of the $\mathbb{GF}$ for the MMS-DES.

A. Calculation of Geometric Factor

Recall that in Sec. II, Eq. (2), we derived a generalized equation describing the number of counts detected (C_{ijk}) in terms of the space–time averaged detector response function ($\bar{\mathbb{R}}_{ijk}$) and the particle distribution function, $f(E, \theta, \phi)$. We were then able to derive a generalized equation for $\mathbb{GF}$ (Eq. (4)) through the integration of $\bar{\mathbb{R}}_{ijk}$. We shall now use this same method to derive an equation for the laboratory based determination of $\mathbb{GF}$.

Our first step is to define a particle distribution function, $f(E, \theta, \phi)$, so that this may be substituted into Eq. (2). Then it will be possible to describe $\bar{\mathbb{R}}_{ijk}$, a notional mathematical construct, in terms of C_{ijk}, a physical measurable quantity, and thus find $\mathbb{GF}$.

The laboratory determination of the geometric factor therefore begins with a direct measurement of the detector response function, obtained by probing the instrument with a collimated quazi-monoenergetic particle beam at various beam energies and angles. In an idealized experiment, the velocity distribution of the beam particles would be a delta function, as below in Eq. (25),

$$f(\boldsymbol{v}) = n_B\, \delta(\mathbf{v} - \mathbf{v_B}), \tag{25}$$

where n_B is the beam density. However, in order to substitute this into Eq. (2), we must now convert this in terms of (E, θ, ϕ) (spherical polar energy coordinates), as below in Eq. (26),

$$f(E, \theta, \phi) = \frac{n_B m^{3/2} E_B^{1/2}}{\sqrt{2}} \frac{\delta(E - E_B)\delta(\theta - \theta_B)\delta(\phi - \phi_B)}{E \cos\theta}, \tag{26}$$

where m is the mass of the particle, E_B is the energy of the beam. Now, by substituting Eq. (26) into Eq. (2), we can describe the ratio of counts detected by the MCP (C_{ijk}) to the *magnitude* of the incident particle flux, Φ:

$$\frac{C_{ijk}}{\Phi} \equiv A_{ij} \cos\theta_B \bar{\mathbb{R}}_{ijk}(E_B, \theta_B, 0; E_0, \theta_0, \phi_0), \tag{27}$$

where A_{ij} is the aperture area and Φ is given below in Eq. (28).

$$\Phi = n_B \left(\frac{2E_B}{m}\right)^{1/2}. \tag{28}$$

Thus, by scanning the particle beam across energy and angle, and by normalizing the resulting MCP count rates by the magnitude of the incident beam flux, it is possible to construct a high resolution image of $\bar{\mathbb{R}}_{ijk}$. Figure 6 shows an example of an instrument response function as measured by the DES-ETU. This shows the variation of normalized counts (C_{ijk}/Φ)

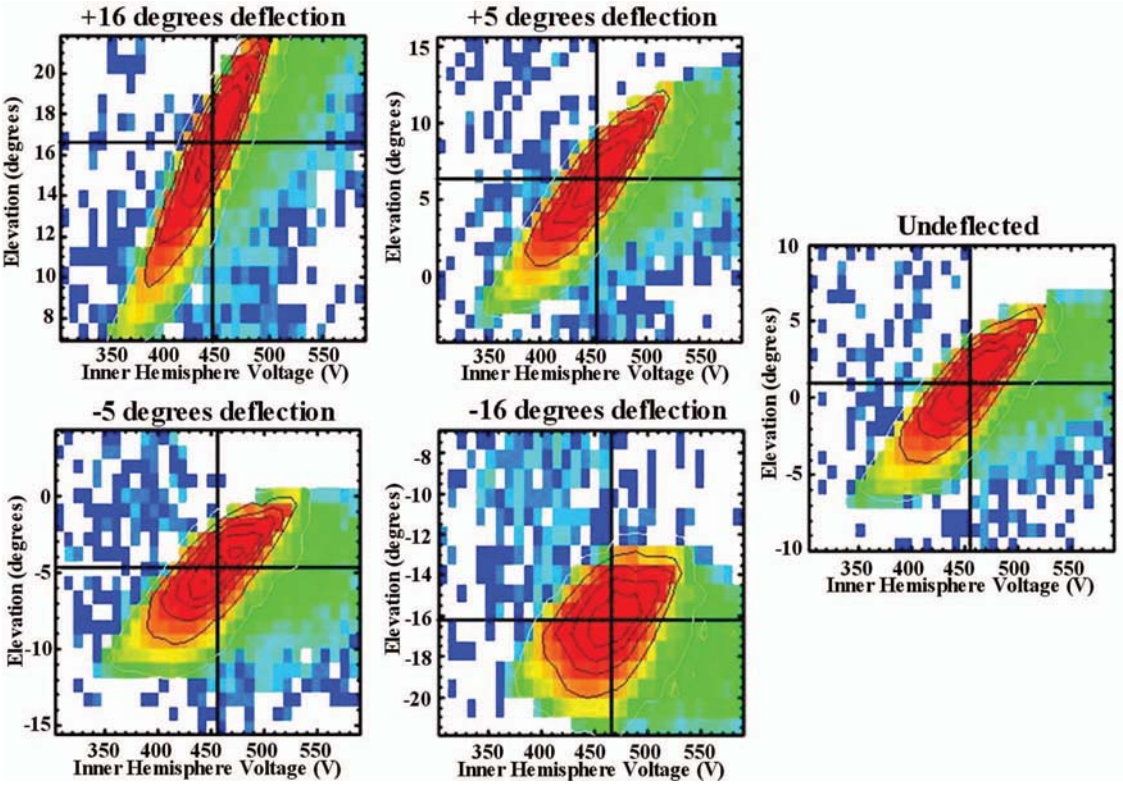

FIG. 6. (Color Online) The response function measured by the Dual Electron Spectrometer engineering test unit (DES-ETU) showing the variation of (C_{ijk}/Φ) over the energy and elevation range for the five deflection states of the instrument.

over the energy and elevation range for the five deflection states of the instrument.

If we again assume that the detector response has the following ϕ dependence (as we did for simulations in Eq. (19)):

$$\bar{\mathbb{R}}_{ijk}(E,\theta,\phi;E_0,\theta_0,\phi_0) = \begin{cases} \bar{\mathbb{R}}_{ijk}\begin{pmatrix} E,\theta,0;\ldots \\ \ldots E_0,\theta_0,\phi_0 \end{pmatrix} & \text{if } (\phi_{\min} < \phi < \phi_{\max}) \\ 0 & \text{otherwise,} \end{cases} \tag{29}$$

where, again, $\Delta\phi \equiv \phi_{\max} - \phi_{\min}$ is the instrument azimuthal pixel width, then the geometric factor (see idealized $\mathbb{GF}$ Eq. (4)) is obtained by numerically integrating the measured response function (27), assuming the form (29) for the ϕ dependence of the response function:

$$\mathbb{GF}_{ijk} \approx \frac{\Delta\phi}{E_0^2}\sum_m\sum_n \frac{C_{ijk}}{\Phi}E_m\cos\theta_n\Delta E_m\Delta\theta_n, \tag{30}$$

where E_m and θ_n are the energies and elevations in the energy-angle scan, ΔE_m is the energy resolution of the scan, $\Delta\theta_n$ is the elevation resolution of the scan, and E_0 is the energy corresponding to the global response maximum in energy-elevation space. Equation (30) should be directly comparable to the simulated geometric factor (24).

B. Error in the laboratory determination of $\mathbb{GF}$

1. Mechanical differences

One potential source of discrepancies between simulation and laboratory determined values of $\mathbb{GF}$ is that of actual physical differences in geometry between the simulation model and the real instrument. The most likely cause of this is either due to incorrect assembly or the accumulation of errors owing to finite tolerances in the engineered assembly. Several studies in the literature have discussed the use of computer simulation to determine how mechanical tolerances affect the performance of an ESA.[1,2,8] The methods used to determine the $\mathbb{GF}$ were different in each study, and vary in degrees of rigor.

2. Determination of the error in $\mathbb{GF}$

Here we give an example of how we have estimated the error in the laboratory determined $\mathbb{GF}$ ($\Delta\mathbb{GF}$), during our characterization of the DES for the MMS mission. Our two main sources of error in the laboratory were the variability in the flux ($\Delta\Phi$), and the poisson statistical error in the count rate (ΔC). We treat these as independent of one another and combine them as given in Eq. (31),

$$\Delta\mathbb{GF} = \sqrt{\left(\frac{\delta\mathbb{GF}}{\delta\Phi}.\Delta\Phi\right)^2 + \left(\frac{\delta\mathbb{GF}}{\delta C}.\Delta C\right)^2}, \tag{31}$$

where the partial differential of $\Delta\mathbb{GF}$ with respect to Φ is given by Eq. (32), and with respect to C by Eq. (33),

$$\frac{\delta\mathbb{GF}}{\delta\Phi} = -\frac{\mathbb{GF}}{\Phi}, \tag{32}$$

$$\frac{\delta\mathbb{GF}}{\delta C} = \frac{\mathbb{GF}}{C}. \tag{33}$$

Thus the error in the $\mathbb{GF}$ of our lab measurements is given by Eq. (34),

$$\Delta\mathbb{GF} = \mathbb{GF}\sqrt{\left(\frac{\Delta\Phi}{\Phi}\right)^2 + \left(\frac{\Delta C}{C}\right)^2}. \tag{34}$$

V. EXAMPLE RESULTS: THE MMS DUAL ELECTRON SPECTROMETER

In Sec. II, we derived a generalized equation for the $\mathbb{GF}$ of an ESA. In Secs. III and IV, we showed how it can be applied to determine the $\mathbb{GF}$ through simulation and laboratory calibration. In this section, we apply these equations to example results from both simulation and laboratory and show that they provide consistent answers.

The instrument for which we give example results is the aforementioned DES-ETU (shown in Figure 1). MMS will consist of four spacecraft flying in close formation to study the physics of magnetic reconnection. DES will be make observations of the critical electron diffusion region, the site where magnetic reconnection occurs. Each spacecraft will carry four DES instruments, each containing two top hat ESAs. Therefore, an unprecedented thirty two identical electron analyzers will be built for MMS, with eight per spacecraft. Together these eight will deliver full-sky (4π), high-resolution (11°) electron plasma velocity distributions every 30ms.

The ETU is a high fidelity non-flight DES unit recently tested at the MMS-DES calibration facility at NASA Goddard Space Flight Center. It was built to be identical to a flight model in every way, apart from the substitution of some commercial parts for radiation-hardened flight-quality electronic components. We present two case studies here, the variation of the $\mathbb{GF}$ with energy, and with deflection angle.

Panel A of Figure 7 shows our first case study: The variation of $\mathbb{GF}$ with energy for the undeflected DES-ETU. The result of the simulation is denoted by a diamond and solid line. This is the idealized geometrical response of the analyzer ($\mathbb{GF}'$ – Eq. (22)). We have assumed that the pure electron-optical response of the instrument will not vary significantly with energy (one of the many advantages of a top-hat ESA), and thus the values of $\mathbb{GF}'$ in Panel A come from a single $\sim$1 keV simulation. To determine $\mathbb{GF}$ (which may be directly compared with laboratory), we have multiplied $\mathbb{GF}'$ (determined through computer simulation) by our value of $q(E)$ (determined in Sec. III C 1, and shown in Figure 5). This simulated value of the $\mathbb{GF}$ is given by the diamonds and dotted line of Figure 7. The results from laboratory calibration are denoted by the stars, with errors calculated using Eq. (34).

This case study shows a variation of $\mathbb{GF}$ that is caused by the detector, and not part of the intrinsic geometrical

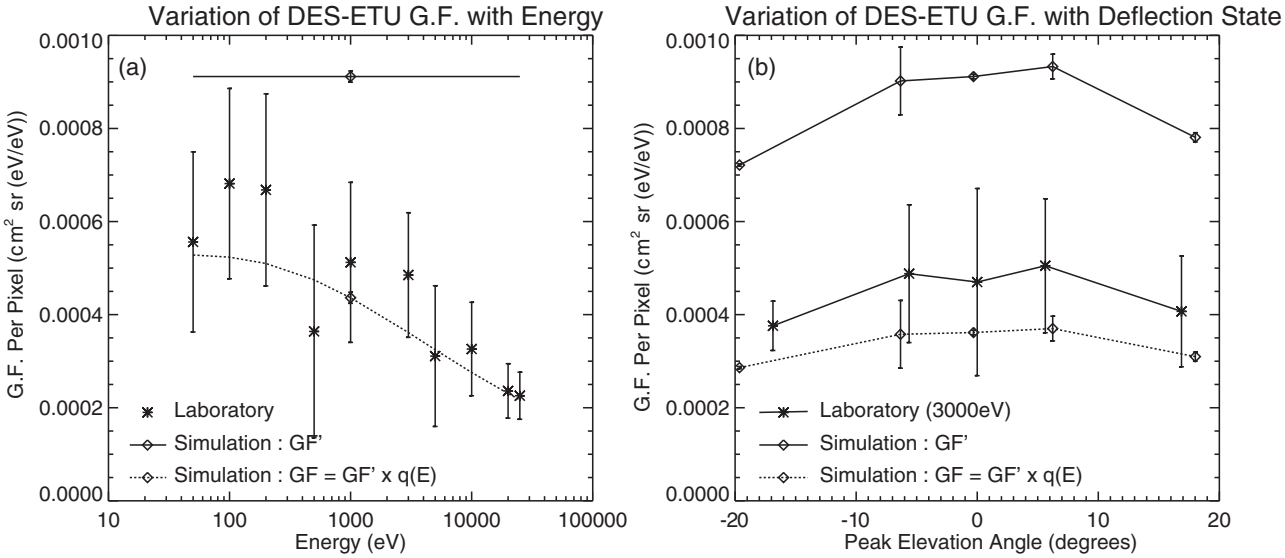

FIG. 7. Showing the variation in geometric factor per pixel for the Dual Electron Spectrometer engineering test unit (DES-ETU) with Energy (panel a) and for each of the five deflection states at 3000 eV (panel b). Raw computer simulation is shown by diamonds and a solid line, computer simulation with estimated q(E) by diamonds and a dashed line, and laboratory results by stars (panel a) and stars and a dashed and dotted line (panel b). Errors are 1σ.

response. Now that we have confidence that the methods used to calculate $\mathbb{GF}$ in simulation and laboratory are mathematically equivalent, it is possible to fully decouple these effects so that they may be studied separately. It also demonstrates the importance of $q(E)$. The good agreement between laboratory and simulation within errors supports the methods and equations described in this paper.

For our second example, we present a case where the variation in $\mathbb{GF}$ is entirely due to the design of the ESA, and not the detector. DES will use electrostatic deflector plates[17,18] to rapidly scan the sky, allowing the FPI instrument suite to fully sample the whole sky much faster than the spin-rate of the spacecraft. Panel B of Figure 7 shows the variation of $\mathbb{GF}$ over the range of deflection angles used on the DES, at a fixed energy of 3 keV, with errors calculated using Eq. (34).

Five sets of simulations were run with different voltages on the deflector plates, covering the whole range of elevations required for DES. The results of the simulation, $\mathbb{GF}'$, are shown by the solid black line in panel B. This was multiplied by the expected value of $q(E)$ at this energy (see Figure 5), and the resulting $\mathbb{GF}$ is denoted by the diamonds and dashed line. Again, laboratory and simulation show agreement within the errors of each. A comparison allows us to confirm that the slight decrease in $\mathbb{GF}$ at the extremes of deflection is an intrinsic property of the electron optics of the ESA. This gives us confidence that we have a good understanding of the electron optical properties of the DES, and in the mechanical fidelity to which the DES-ETU was constructed, giving us a firm foundation for moving into construction of the flight units.

VI. CONCLUSIONS

Increasingly, particle simulations are playing an essential role in the design and calibration of electrostatic analyzers, facilitating the identification, and mitigation of the many sources of systematic error present in laboratory calibration. Of particular interest is the geometric factor, a vital parameter that allows counts on the detector to be related to incident differential particle flux. Often, however, simulations and calibration experiments are carried out under substantially different assumptions and conditions, making comparisons of simulated and measured detector characteristics very challenging.

In this paper, we derived expressions from first principles for the simulated and measured geometric factors and discussed how errors may be estimated in both cases. Then we gave examples of how these were applied as part of the design and calibration of the new Dual Electron Spectrometer (DES) being developed at NASA Goddard Space Flight Center for NASA's Fast Plasma Investigation (FPI) of the upcoming *Magnetospheric Multiscale* (MMS) mission.

Our laboratory measurements show that the $\mathbb{GF}$ per pixel decreases with energy between $\approx 5.6 \times 10^{-4}\,\mathrm{cm^2\,sr\,(eV/eV)}$ at 50 eV to $\approx 2.3 \times 10^{-4}\,\mathrm{cm^2\,sr\,(eV/eV)}$ at 25 keV due to the change in efficiency of the MCP. Our error (1σ) in the measurement of the $\mathbb{GF}$ per pixel also decreases with energy from $\pm 3.9 \times 10^{-4}\,\mathrm{cm^2\,sr\,(eV/eV)}$ at 50 eV to $\pm 1.0 \times 10^{-4}\,\mathrm{cm^2\,sr\,(eV/eV)}$ at 25 keV due to the flux of the electron gun being more stable (lower $\Delta\Phi$) at higher energies. The $\mathbb{GF}$ of the DES decreases at the $\pm 16.875^\circ$ deflection angles due to obscuration of field of view by the DES deflector plates themselves. We wish to note that this will not be the first instrument to fly with this feature,[16] and since the decrease is small (especially when compared to the error of the measurement), we do not expect it to hamper scientific return.

The overall agreement of $\mathbb{GF}$ independently determined through both laboratory and simulation give us confidence that the techniques presented in this study are mathematically rigorous and will give consistent results in comparing simulations and measurements. This provides clarity on a matter for which there was clear and pressing need and offers a firm foundation for all future investigations of space plasmas. We have been applying this formalism to the DES flight model

(currently under construction) and these results will be presented in a future DES instrument paper.

ACKNOWLEDGMENTS

This work was supported by an appointment to the NASA Postdoctoral Program at NASA Goddard Space Flight Center, administered by Oak Ridge Associated Universities through a contract with NASA. We also wish to thank the following members of the DES-ETU team who contributed to this paper through mechanical design, electronics design and testing, test software development, and assembly and testing of the ETU: Craig Auletti, Victor Bigio, Will Burrows, Nga Cao, Kent Christian, Nick Galassi, Kelvin Garcia, Jacob Haseman, Art Jaques, Joe Kajowski, Carol Lilly, Jim Lobell, Quang Nguyen, Lillian Reichenthal, Traci Rosnack, Alan Rucker, Chad Salo, Darrell Smith, David Steinfeld, Kimathi Tull, and Mike Zeuch.

[1]M. Wuest, D. Evans, and R. V. Steiger, ISSI Scientific Report **SR-007**, 2007.
[2]J. H. Vilppola, J. T. Keisala, P. J. Tanskanen, and H. Huomo, Rev. Sci. Instrum. **64**, 2190 (1993).
[3]T. J. M. Zouros, O. Sinse, F. M. Spiegelhalder, and D. J. Manura, Int. J. Mass. Spectrom **261**, 115 (2007).
[4]D. J. Knudsen *et al.*, Rev. Sci. Instrum. **74**, 202 (2003).
[5]A. D. Johnstone *et al.*, J. Phys. E **20**, 795 (1987).
[6]L. M. Chase, Rev. Sci. Instrum. **44**, 998 (1973).
[7]C. W. Carlson, D. W. Curtis, G. Paschmann, and W. Michel, Adv. Space Res. **2**, 67 (1982).
[8]G. A. Collinson *et al.*, Meas. Sci. Technol. **20**, 055204 (2009).
[9]R. D. Woodliffe and A. D. Johnstone, *Measurement Techniques in Space Plasmas – Particles*, edited by R. F. Pfaff, J. E. Borovsky, and D. T. Young, 1998, p. 263.
[10]G. A. Collinson and D. O. Kataria, Meas. Sci. Technol. **21**, 105903 (2010).
[11]U. Rohner *et al.*, Meas. Sci. Technol. **23**, 025901 (2012).
[12]R. L. Kessel, A. D. Johnstone, A. J. Coates, and R. A. Gowen, Rev. Sci. Instrum. **60**, 3750 (1989).
[13]C. W. Carlson and J. P. McFadden, *Measurement Techniques in Space Plasmas – Particles*, edited by R. F. Pfaff, J. E. Borovsky, and D. T. Young, 1998, pp. 125–+.
[14]J. L. Wiza, Nucl. Instrum. Methods **162**, 587 (1979).
[15]A. D. Johnstone *et al.*, Space Sci. Rev. **79**, 351 (1997).
[16]J. Sauvaud *et al.*, Space Sci. Rev. **136**, 227 (2008).
[17]D. T. Young *et al.*, Space Sci. Rev. **129**, 327 (2007).
[18]O. L. Vaisberg *et al.*, *Complex Plasma Analyzer SCA-1* (RKA-IKI-CESR-CNES, 1995), pp. 170–177.
[19]K. W. Ogilvie *et al.*, Space Sci. Rev. **71**, 55 (1995).
[20]G. R. Lewis *et al.*, Planet. Space Sci. **58** (2010).
[21]A. N. Fazakerley, S. J. Schwartz, and G. P. Paschmann, Analysis Methods for Multi-Spacecraft Data **1**, 91 (2000).
[22]J. P. McFadden and C. W. Carlson, *Measurement Techniques in Space Plasmas – Particles*, edited by R. F. Pfaff, J. E. Borovsky, and D. T. Young, 1998, pp. 249–+.
[23]R. D. Woodliffe, "Design of space borne plasma analysers by computer simulation," Ph.D. dissertation (Mullard Space Science Laboratory, Department of Physics and Astronomy, University College London, 1991).
[24]G. A. Collinson, "The computer simulated design of an improved plasma analyser towards an electron spectrometer for solar orbiter," Ph.D. dissertation (Mullard Space Science Laboratory, Department of Physics and Astronomy, University College London, 2010).
[25]F. Allegrini *et al.*, Rev. Sci. Instrum. **80**, 104502 (2009).
[26]J. P. McFadden *et al.*, Space Sci. Rev. **141**, 277 (2008).
[27]F. Bordoni, Nucl. Instrum. Methods **97**, 405 (1971).
[28]H. C. Straub, M. A. Mangan, B. G. Lindsay, K. A. Smith, and R. F. Stebbings, Rev. Sci. Instrum. **70**, 4238 (1999).
[29]R. R. Goruganthu and W. G. Wilson, Rev. Sci. Instrum. **55**, 2030 (1984).
[30]R. S. Gao, P. S. Gibner, J. H. Newman, K. A. Smith, and R. F. Stebbings, Rev. Sci. Instrum. **55**, 1756 (1984).
[31]N. Kishimoto, M. Nagamine, K. Inami, Y. Enari, and T. Ohshima, Nucl. Instrum. Methods Phys. Res. A **564**, 204 (2006).
[32]L. Austin and H. Starke, Ann. Phys. Lpz. **9**, 271 (1902).
[33]E. Rudberg, Proc. R. Soc. London **A127**, 111 (1930).
[34]H. Bruining, *Physics and Applications of Secondary Electron Emission* (Pergamon, New York, 1954).